Science Advances

AAAS

advances.sciencemag.org/cgi/content/full/3/7/e1700842/DC1

Supplementary Materials for

Fluorinated h-BN as a magnetic semiconductor

Sruthi Radhakrishnan, Deya Das, Atanu Samanta, Carlos A. de los Reyes, Liangzi Deng, Lawrence B. Alemany, Thomas K. Weldeghiorghis, Valery N. Khabashesku, Vidya Kochat, Zehua Jin, Parambath M. Sudeep, Angel A. Martí, Ching-Wu Chu, Ajit Roy, Chandra Sekhar Tiwary, Abhishek K. Singh, Pulickel M. Ajayan

Published 14 July 2017, *Sci. Adv.* **3**, e1700842 (2017)
DOI: 10.1126/sciadv.1700842

This PDF file includes:

- References (*36–57*)

section S1. Synthesis

1a. Solvothermal Synthesis

For the synthesis of Fluorinated Boron Nitride (F-BN), 30mg of hexagonal Boron Nitride (h-BN) was dispersed in 30mL of the mixture of Nafion and N, N Dimethyl Formamide (DMF). The mixture is sealed in an autoclave and heated at 200°C for 12 hours. The time of the reaction was found to be important to control the amount of fluorination. A longer time of synthesis yielded higher fluorination. The temperature and pressure were also found to be critical parameters in the fluorination. The choice of solvent was also found to be a deciding factor as the use of other solvents were not found to yield good results. After the synthesis the sheets that settle to the bottom was washed with acetone. The washing removes any excess polymer which remain between the sheets of the F-BN. After washing, the removal of the polymer is completed by an annealing at 200°C for 24 hours. More than 80% yield of F-BN could be obtained by this method.

A visible change is observed in h-BN on fluorination. The white powder acquires a brownish tint. This is evidently due to absorption in the visible range due to a decrease in the bandgap. It is also observed in amine functionalization of h-BN (**10**).

1b. Direct Fluorination by F_2 Gas

In this method a mixture of Helium and fluorine gas is used as the precursor for fluorination. Commercial h-BN is taken in a Monel reactor and the fluorination is performed at 100°C for 1-hour and 5-hours respectively. The 1-hour yields lower fluorine content in the sample while the 5 hour yields much higher fluorine. However due to the high reactivity of fluorine, it leads to etching of the reactor walls leading to some metallic contamination in the samples.

At the low fluorination, the structural characteristics were found to be similar to the fluorination product obtained by using solvothermal method (fig. S1). At higher fluorination B-F_2 and N-F_2 signals were also found in the XPS results (fig. S2).

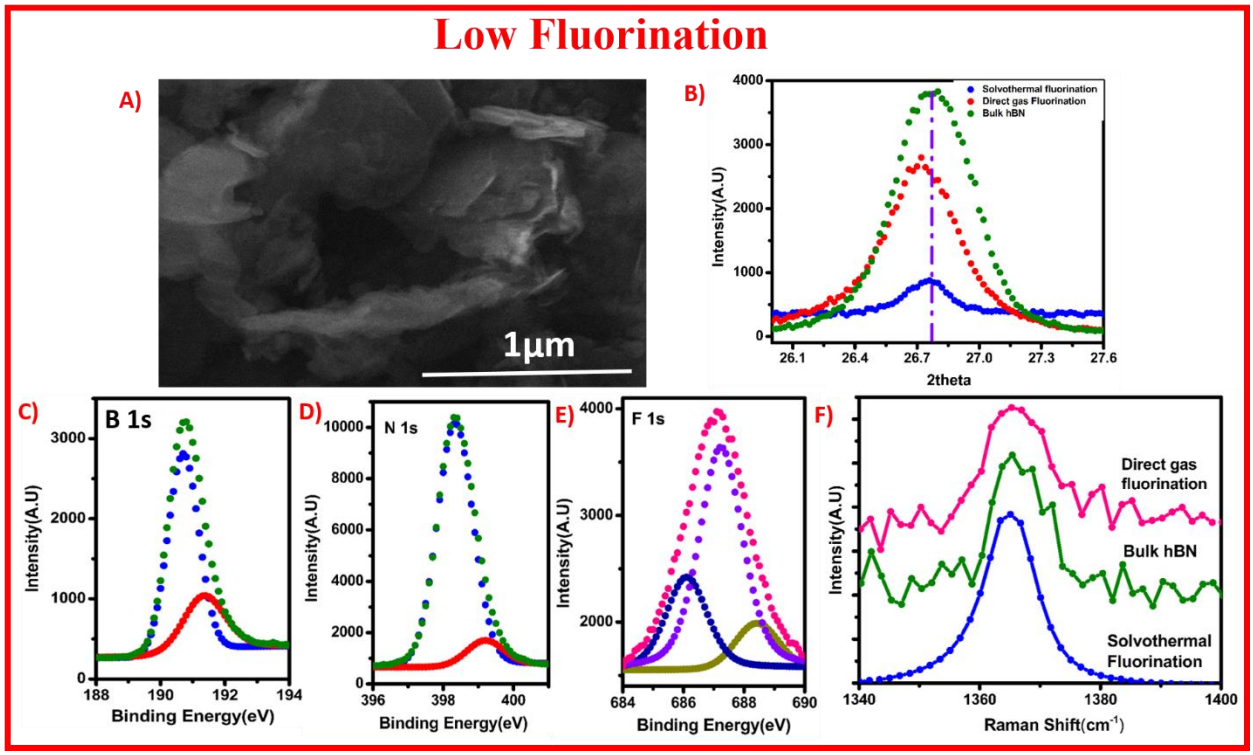

fig. S1. Structural characterizations of plasma-fluorinated boron nitride. (**A**) Scanning Electron Micrograph shows the layered structure. (**B**) X-ray Diffraction revealing a small shift to the lower angle (**C**) De-convoluted X-ray Photoelectron spectra of B1s and (**D**) N 1s (**E**) F1s (**F**) overlapped Raman spectra of pure h-BN and h-BN fluorinated by both the methods.

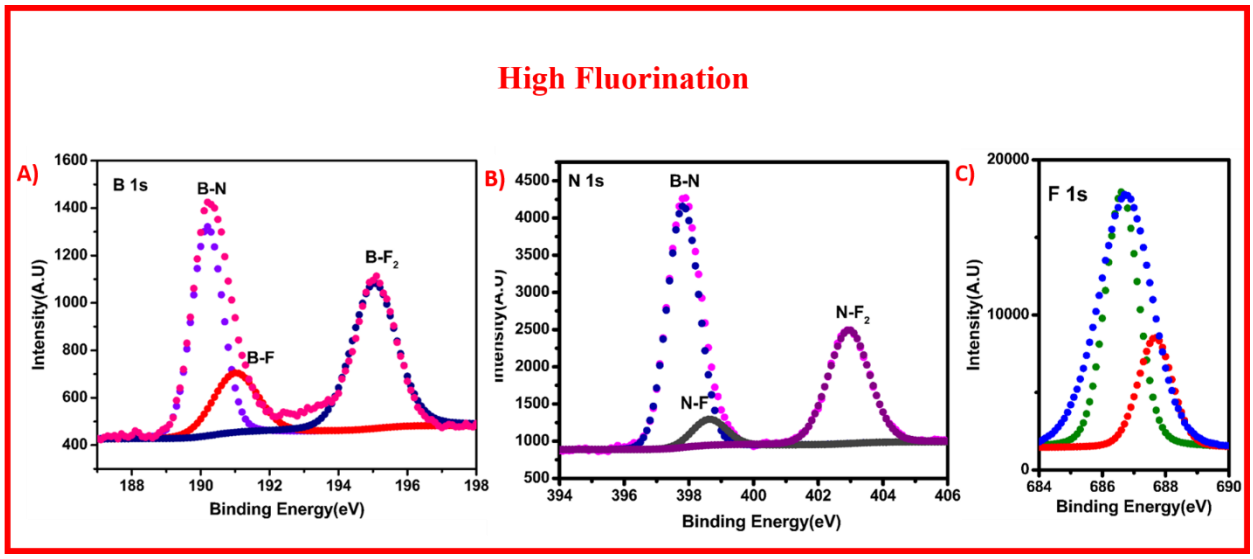

fig. S2. XPS spectrum of highly fluorinated boron nitride. De-convoluted high-resolution X-ray Photoelectron spectra of (**A**) B1s and (**B**) N 1s (**C**) F 1s F-BN obtained by 5-hours plasma fluorination.

section S2. ^{19}F NMR analysis

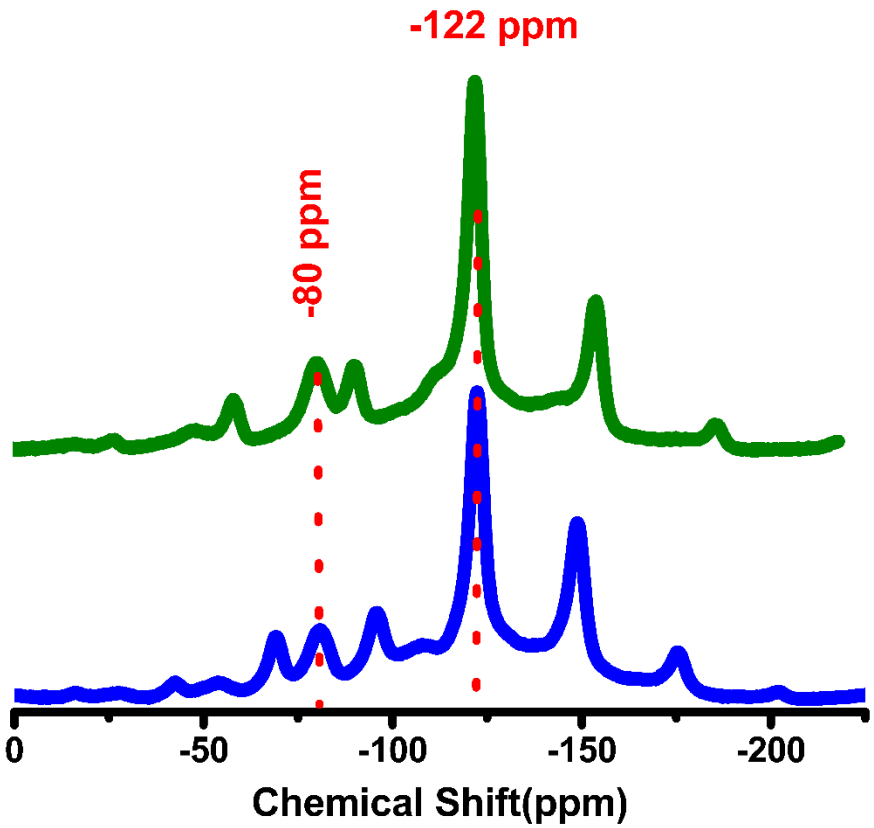

fig. S3. ^{19}F MAS spectra (376.3-MHz) of F-BN with MAS rate of 12 and 10 kHz. The two centerbands belonging to two different fluorine environments are labeled. The other peaks are spinning sidebands.

Preliminary MAS ^{19}F NMR studies were done at 376 MHz with spinning speeds up to 12 kHz (4 mm diameter rotor). The spectra indicate the presence of at least two centerband signals (at -122 and -80 ppm, relative to $CFCl_3$ defined as 0 ppm and where the negative sign indicates a still more shielded environment) for a sample prepared by solvothermal treatment of h-BN with Nafion in DMF. The numerous spinning sidebands from relatively slow spinning and probe background signals prevent a definitive interpretation of the ^{19}F signals. Additional work is planned with much faster spinning at a different field strength so that all of the ^{19}F centerband signals can be clearly recognized.

Securely assigning ^{19}F signals to F-BN and differentiating N-F signals from B-F signals pose significant challenges. As will be briefly discussed, there are no good model systems with ^{19}F chemical shift data for F-BN, and ^{19}F chemical shifts are very sensitive to structural changes. A set of cyclic compounds of the type cyclo-[BF-NZ]$_3$ (Z = H, CH_3, *n*-C_3H_7) exhibits ^{19}F chemical shifts from -127 to -131 ppm (relative to $CFCl_3$ defined as 0 ppm) (**36**). A compound with fused 4- and 5-membered rings containing only boron and nitrogen exhibits an ^{19}F chemical shift for the FBN_2 group at -157 ppm, while this and a closely related compound exhibit ^{19}F chemical shifts for the $F_2BN_2^-$ group at -158 ppm (**37**).

There appear to be relatively few compounds differing only in the replacement of nitrogen with boron for which ^{19}F chemical shifts of the N-F and B-F groups have been reported (**table S1**). While the first 6 entries clearly show that replacing nitrogen with boron exerts a large shielding effect on ^{19}F, the last 2 entries show a modest deshielding effect. Thus, assigning ^{19}F signals to N-F or B-F environments on the basis of chemical shift requires caution.

table S1. Literature of ^{19}F chemical shifts of B-F and N-F.

Compound	Chemical Shift (ppm)	Reference	Compound	Chemical Shift (ppm)	Reference
NF_3	146.9	(**38**), p 499	BF_3	-126.8	(**38**), p 407
NF_2Cl	141.5	(**38**), p 499	BF_2Cl	-79.8	(**38**), p 408
$NF_2C_2H_5$	52	(**38**), p 506	$BF_2C_2H_5$	-74.6	(**38**), p 408
NF_2H	-11.2	(**38**), p 499	BF_2H	-68.5	(**38**), p 408
NF_2-NF_2	60.4	(**38**), p 506	BF_2-BF_2	-50.0	(**38**), p 408
$NFCl_2$	128	(**38**), p 499	$BFCl_2$	-32.3	(**38**), p 408
$NF(CH_3)_2$	-24.5	(**38**), p 503	$BF(CH_3)_2$	-19.3	(**38**), p 408
$NF(C_2H_5)_2$	-53.0	(**38**), p 504	$BF(C_2H_5)_2$	-32.8	(**38**), p 408

[a] Relative to $CFCl_3$ defined as 0 ppm (negative sign indicates a still more shielded environment).

There appear to be just two examples (**table S2**) with ^{19}F NMR data for fluorinating a FNXY compound to make an F_2NXY^+ cation (analogous to fluorinating nitrogen in h-BN). The extreme sensitivity of the ^{19}F chemical shift to the number of fluorine atoms in the cation is shown by a

further large increase in shielding (to about -113 ppm) for NH_3F^+ in a wide variety of salts (**39-41**) (The NHF_3^+ cation has apparently not yet been isolated in the condensed phase.(**42**)).

table S2. Literature of ^{19}F chemical shifts of FNXY and F_2NXY.

Compound	Chemical Shift (ppm)	Reference	Compound	Chemical Shift (ppm)	Reference
NF_3	146.9	(**38**), p 499	NF_4^+	~ 216[b]	(**43-45**)
NH_2F	-155.6	(**38**), p 497	$NH_2F_2^+$	11.6	(**39**)

[a] Relative to $CFCl_3$ defined as 0 ppm (negative sign indicates a still more shielded environment).

[b] There is only a slight dependence of the chemical shift on the anion present.

In contrast, fluorinating an FBXY compound to make an F_2BXY^- anion (analogous to fluorinating boron in h-BN) usually results in further shielding of the ^{19}F signal (**table S3**), with the anionic chemical shifts ranging from -88 ppm to -151 ppm in six simple inorganic examples. In contrast, going from $FB(C_6F_5)_2$ to $F_2B(C_6F_5)_2^-$ has a -31 ppm deshielding effect, with the anion at -145 ppm. The data in tables S1 and S3 show that the presence of two organic groups results in a very different change in the ^{19}F chemical shift upon replacing N with B (**table S1**) or upon generating the anion (**table S3**).

table S3. Literature of ^{19}F chemical shifts of FBXY and F_2BXY.

Compound	Chemical Shift (ppm)	Reference	Compound	Chemical Shift (ppm)	Reference
BF_3	-126.8	(**38**), p 407	BF_4^-	-151.3	(**38**), p 411
BF_2Cl	-79.8	(**38**), p 408	BF_3Cl^-	-124.6	(**38**), p 411
BF_2Br	-62.9	(**38**), p 403	BF_3Br^-	-113.8	(**38**), p 411
$BFCl_2$	-32.3	(**38**), p 408	$BF_2Cl_2^-$	-104.1	(**38**), p 411
$BFBr_2$	-0.9	(**38**), p 403	$BF_2Br_2^-$	-88.2	(**38**), p 411
BFClBr	-16.5	(**38**), p 408	BF_2ClBr^-	-95.7	(**46**)
$BF(C_6F_5)_2$	-176	(**38**), p 408	$BF_2(C_6F_5)_2^-$	-144.6	(**38**), p 412

[a] Relative to $CFCl_3$ defined as 0 ppm (negative sign indicates a still more shielded environment).

Samples of fluorinated h-BN prepared by different methods will subsequently be studied by very fast MAS ^{19}F NMR to gain additional insights. Because the typical stator in the NMR probe is made of boron nitride and thus would give very strong boron and nitrogen background signals, it would be very difficult to unambiguously detect any boron or nitrogen signals from B-F or N-F groups in the F-BN sample.

section S3. Structural characterizations

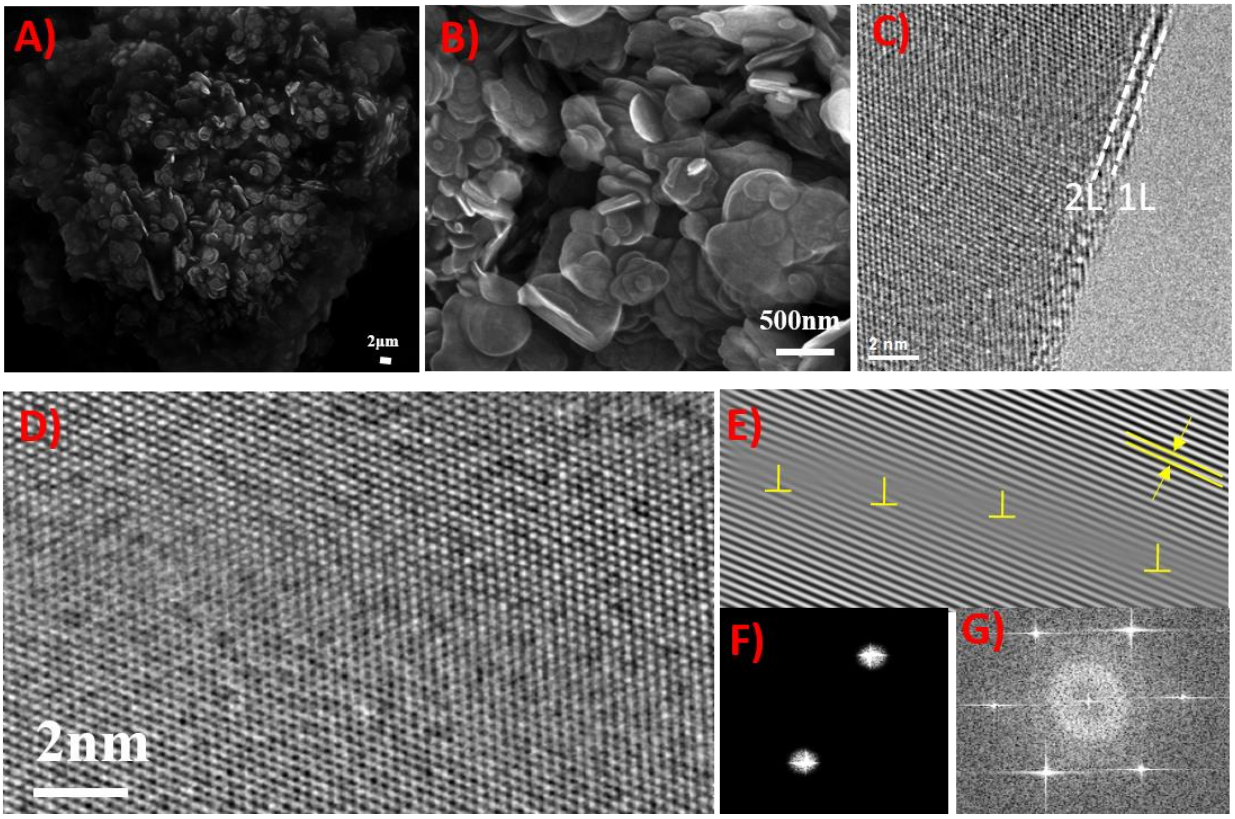

fig. S4. Electron microscope images of the fluorinated boron nitride sheets. (**A**) Low Magnification and (**B**) High magnification SEM image of F-BN showing the flower-like morphology as seen in h-BN. (**C**) HRTEM images at the edge of the sheet to show the number of layers. (**D**) HRTEM images of the inside part of an F-BN sheet (**E**) Inverse FFT image using selective spot from (**F**) Selected spot of the (**G**) FFT image, depicting defect.

The detailed SEM and TEM characterization is performed to understand the effect of fluorination and defects introduced in the lattice. The low magnification SEM micrograph shown in fig. S4(A) reveals a uniform size distribution. The high magnification image (fig. S4(B)) shows circular morphology of F-BN sheet as observed in exfoliated sheets of h-BN (**47**). These thin sheets are found to be single or bilayers as shown in the HRTEM image of the edge of the sheet (fig. S4(C)). The HRTEM image of the sheet interior shows single oriented sheets without any boundary or other impurity (fig. S4(D)). The lattice spacing is found to be 0.2 nm, which is consistent with h-BN 001 lattice arrangements. The FFT of the area shows hexagonal symmetry with 001 orientation. The inverse FFT of the two spots shows the presence of defects in F-BN (fig. S4(G)).

section S4. Bandgap calculations

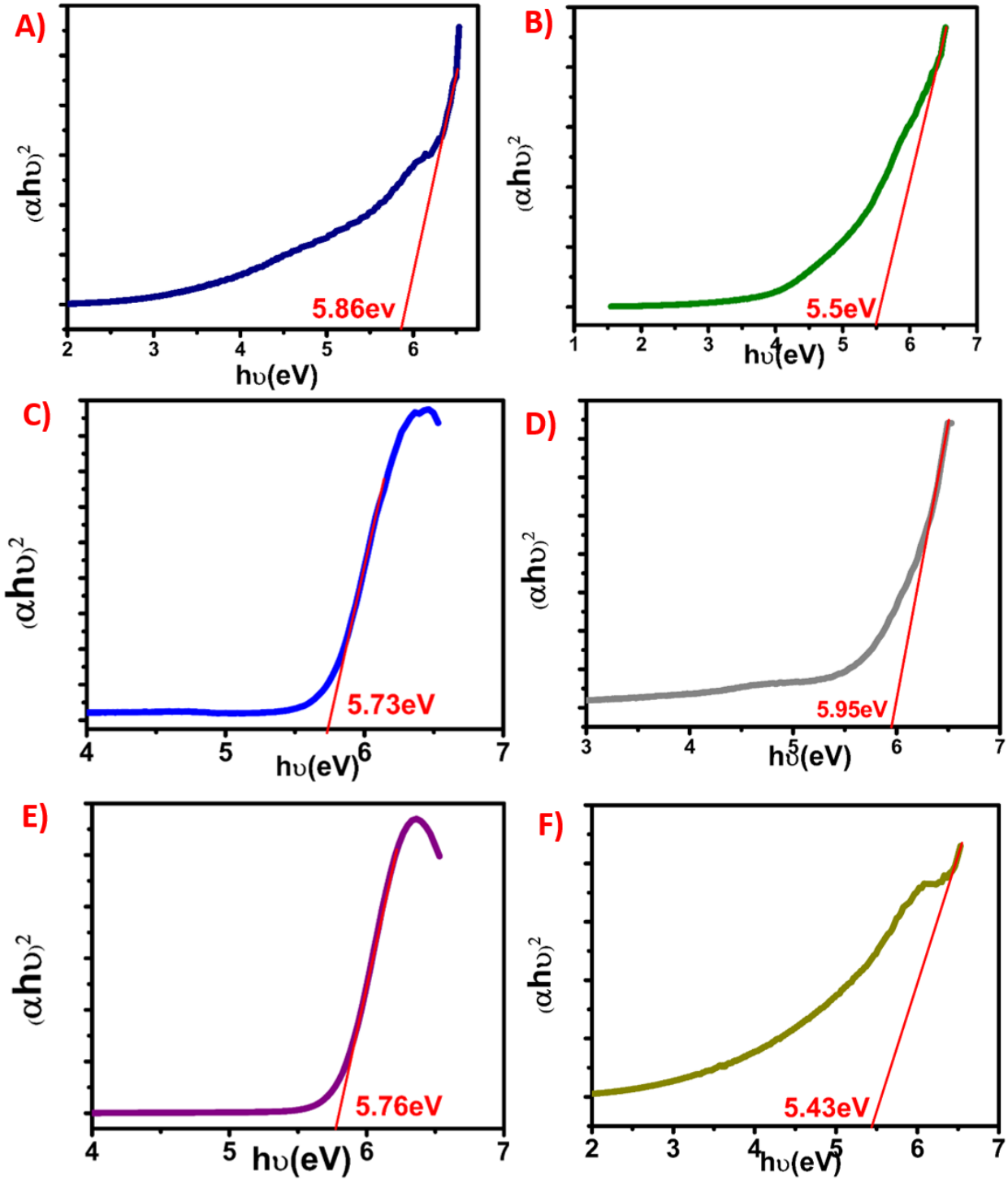

fig. S5. Tauc plot for the various doping of h-BN sheets. (**A**) h-BN (**B**) 3.2% F doped h-BN (**C**) 8.1% F doped h-BN (**D**) 10.6% F doped h-BN (**E**) 11.3% F doped h-BN (**F**) 13.2% F doped h-BN

The band gap was calculated from the absorption measurements. Absorption coefficient (α) was calculated from the values of absorption (A) using the formula 2.303A/L where L is the path length. Tauc plot is constructed between $(\alpha h\upsilon)^2$ and hυ, and a tangent to the linear region of the Tauc plot is extrapolated to meet the X-axis. The value of energy where the tangent meets the X-axis is the bandgap. The samples were mildly sonicated in water and centrifuged at low speed to obtain the supernatant for the analyses.

section S5. Photoluminescence spectra

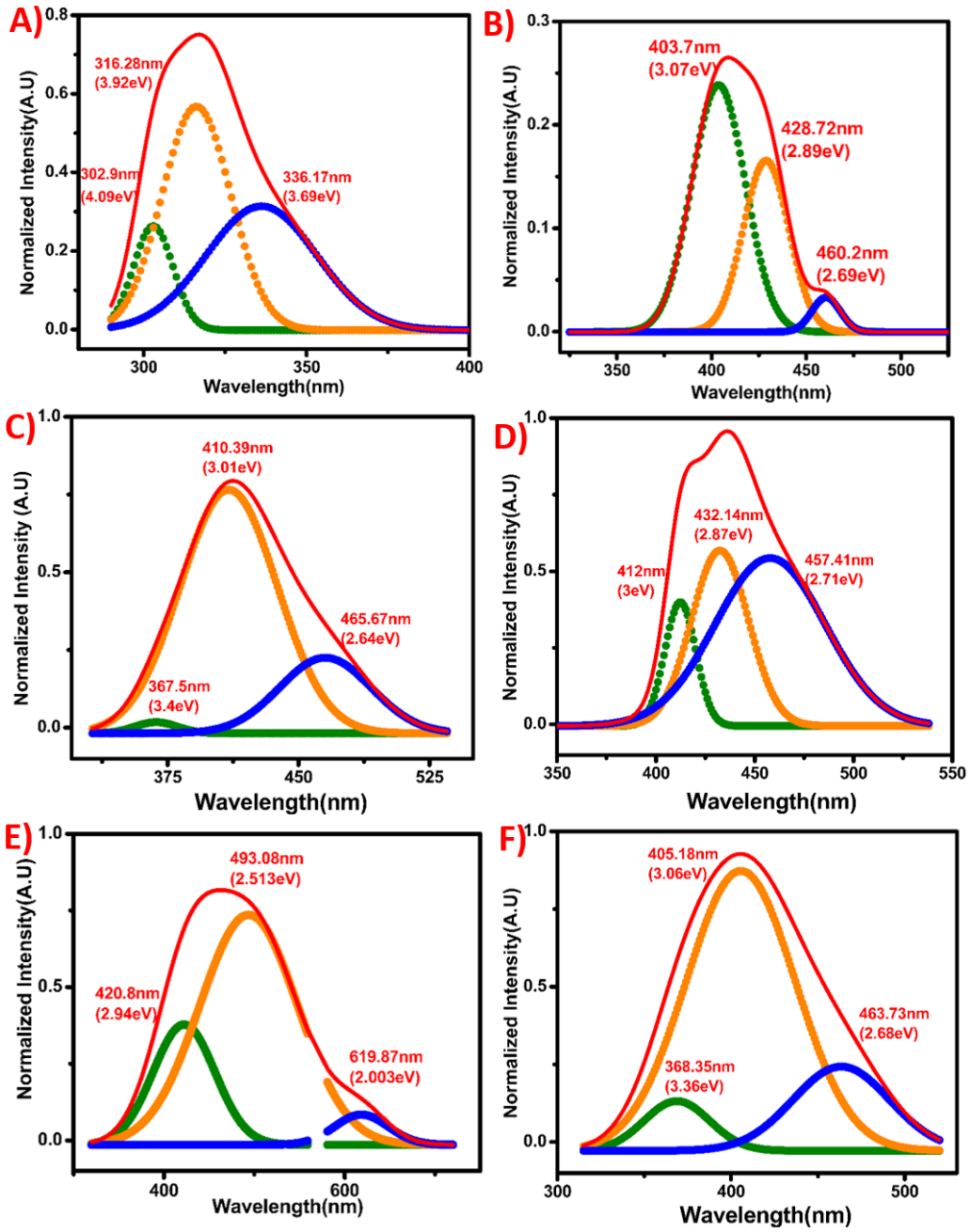

fig. S6. Emission spectra for the different doping concentrations of the fluorine in boron nitride nanosheets on excitation at 280 nm. (**A**) pure hBN (**B**)3.2% F doped h-BN (**C**) 8.1% F doped h-BN (**D**) 10.6 F doped h-BN (**E**) 11.3% F doped h-BN, the discontinuity is due second order diffraction which is subtracted for the entire spectrum (**F**) 13.2% F doped h-BN

The PL spectra were obtained by dispersing the samples in water and were excited at 280 nm. The sample with 11.3% Fluorine (fig. S6(E)), seemed to have a wider range of emission, a cuvette made of PMMA cuvette (BRAND) was placed before the detector in order to decrease the second order diffraction, functioning as a filter; such cuvette has an emission right at 622 nm (fig. S7). The emission of the cuvette by itself was measured under the same conditions and subtracted from the original spectrum, causing the small shoulder at this point.

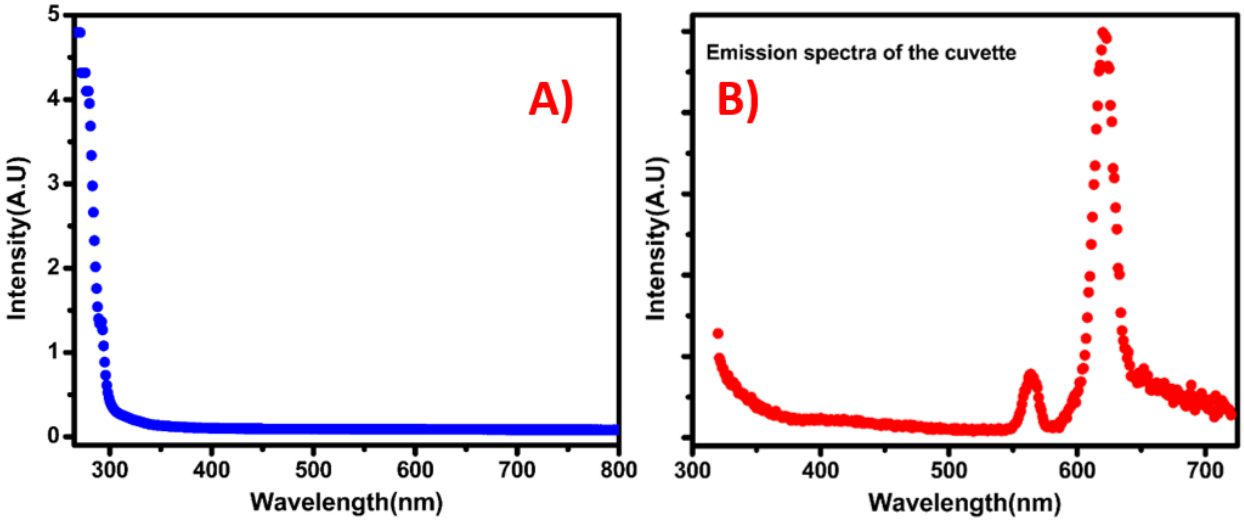

fig. S7. Control measurements of the blank cuvette. (**A**) Absorption spectra and (**B**) Emission spectra under the same excitation wavelength

In the pure hBN samples the first two peaks have an energy gap corresponding to the phonon energy in hBN. The peak at 4.09 eV (fig. S7(A)) is the zero phonon line corresponding to TO phonons. The phonon replica of this peak is observed at 3.92 eV (w_{TO} = 169 meV) (**48**). The peak at 3.69 eV however cannot be assigned to a phonon replica. It could arise from the Carbon impurities in the sample (**20**).

At the lowest doping concentration of 3.2% the energy gap between the peaks suggest the effects from phonon interactions which is then seen at 10.6% doping only. However the phonon energy at this high level of doping corresponds to cubic BN which is most likely due to the increase in number of defects with subsequent fluorination, causing the bonding to change from sp^2 to sp^3 (**49**). At the intermediate doping of 8.1% the PL peaks cannot be ascribed to known phonon

modes in hBN, therefore, a defect state introduced by the doping between the valance and conduction band might be contributing to the observed emission. From these observations we deduce that; a defect level is seen only at doping above 5%.

section S6. Magnetic measurements

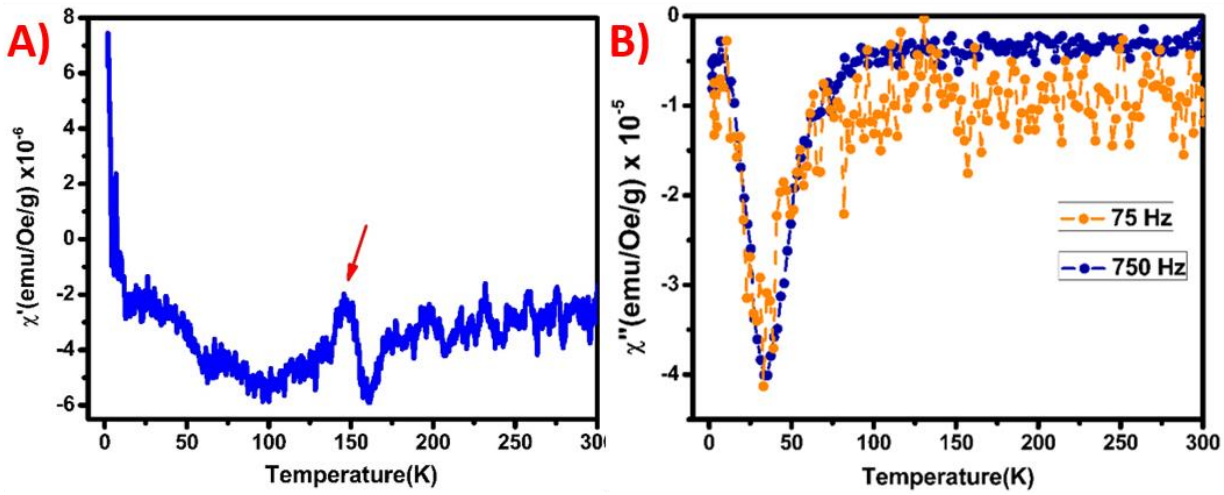

fig. S8. ac magnetic measurements. (**A**) The real part of susceptibility is plotted against the temperature. The ac measurement is conducted at frequency 79Hz. (**B**) The imaginary part of susceptibility against temperature for frequencies 75Hz and 750Hz.

Room temperature hysteresis measurements and DC ZFC-FC from 300K to 2K were carried out in the sample. The ZFC-FC measurement was fitted using curie-weiss law

$$\chi = \chi_D + \frac{C}{T - \theta}$$

Where χ is the observed susceptibility, $\chi_D$is diamagnetic susceptibility, C is Curie constant, T is the measured temperature and θ is Weiss constant. On fitting the measured value with this equation, θ is observed to be -4.7 K. Negative value of θ is commonly observed in the case of anti-ferromagnetic materials.

AC magnetic measurements are done in the temperature range from 2 K to 300 K. A DC bias field of 500 Oe, and ac field of 2 Oe were used for the measurements. It was performed at two different frequencies, 75 Hz and 750 Hz. A small peak at 75 Hz was observed which was not

seen in the high frequency measurement. The existence of this peak was confirmed by another measurement at 79Hz, which is plotted in fig. S8.

section S7. Computational methodology

Theoretical calculations were performed using first principles based density functional theory (DFT) as implemented in Vienna *ab-initio* simulation package (VASP) (**50, 51**). Electron-ion interactions were described using all-electron projector augmented wave (PAW) pseudopotentials (**52**)and Perdew-Burke-Ernzerhof (PBE) generalized gradient approximation (**53, 54**) (GGA) was used to approximate electronic exchange and correlation. In order to model fluorinated BN sheets, 4×4×1 supercell of hBN structure is considered. The fluorinated BN sheets are separated by 15 Å vacuum to avoid spurious interactions between the periodic images. The Brillouin zone has been sampled using Monkhorst-Pack (MP) scheme, 9×9×1 k-grid is used for relaxation calculations. A conjugate gradient scheme is used to relax the structures until the component of forces on each atom were ≤0.005 eV/Å. The electronic wave functions were represented by plane wave basis set with kinetic energy cutoff of 400 eV to ensure the accuracy of the results.

The formation energy values per attached F atom for different concentrations have been calculated using the equation

$$E_{form} = (E_{BN-F} - E_{BN} - (n*E_F)) / n$$

Where E_{BN-F}, E_{BN} and E_F are total energy of BN sheet with attached n number of F atoms, total energy of BN sheet without F atoms and the cohesive energy of F atom.

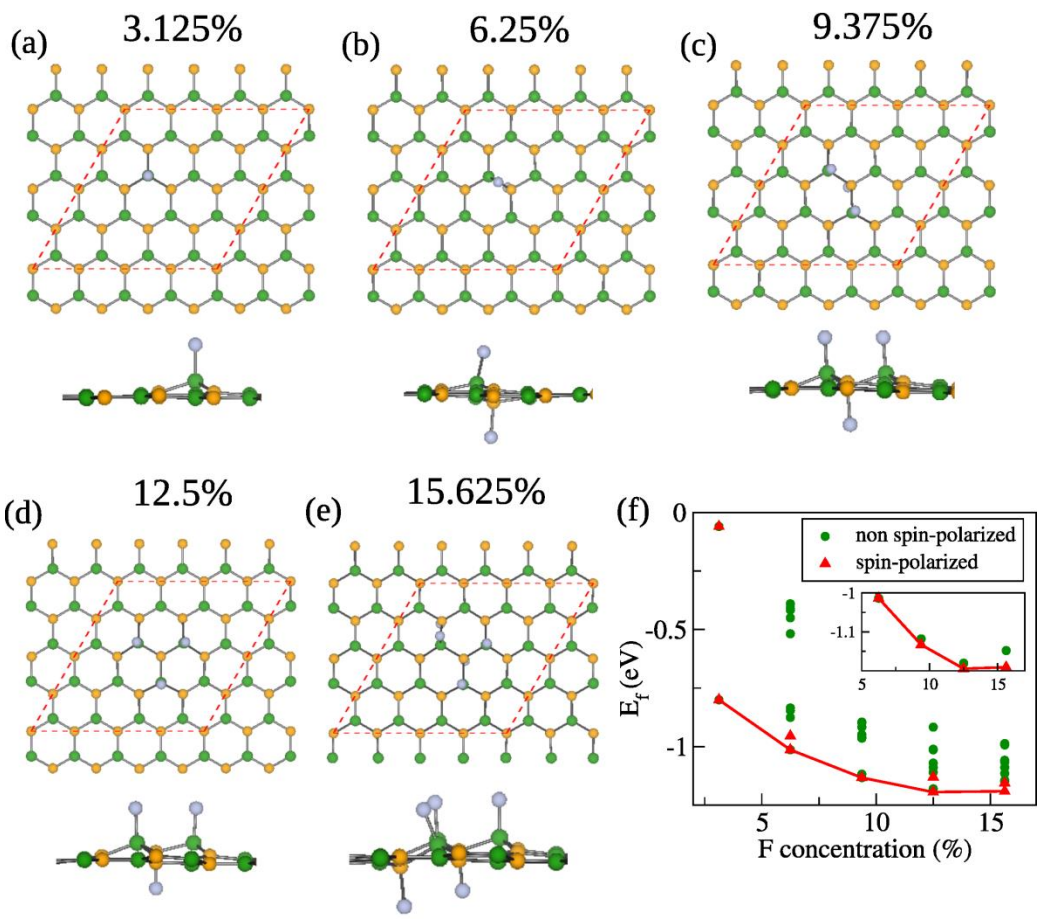

fig. S9. Structures of fluorinated BN sheets. (**A-E**) with different F concentrations where green, orange and blue circles denote B, N and F atoms. (**F**) Plot of formation energies for both non-spin polarized and spin-polarized states as a function of F concentration. Inset of (F) shows the lowest formation energy values for higher F concentration.

The hBN sheet is functionalized with fluorine (F) atoms up to 15.625% doping by considering various symmetrically non-equivalent positions. In a perfect BN sheet, due to the higher electronegativity of nitrogen (N) atom as compared to boron (B), the electron density is shifted towards Nitrogen making the B-N bond polar. Consequently, all the N atoms gain partial negative charge. Due to this electron deficiency at B site along with the higher electronegativity difference between F and B, the first F atom prefers to attach to electropositive B as shown in fig. S9(A). Bader charge analysisreveals that after first F bond with a B, F atom gains 0.93 electronic charge (**55-57**). A significant part of this charge in the F atom comes from the three

closest N atoms, which lose a net electronic charge of ~0.46 and the remaining come from other N atoms. Therefore, the next F atom attaches to one of these three nearest N atoms on the opposite side of the hBN sheet as depicted in fig. S9(B). The addition of second fluorine corresponds to 6.25% F concentration in the unit cell under consideration. While the F atom attached to electropositive B atom takes 0.94 electronic charge, F attached to N takes 0.36 electronic charge, which indicates B-F bonds are more polar compared to the F-N bonds. The calculated binding energy of F-B bond is -0.8 eV, which is significantly larger compared to the binding energy of -0.05 eV for F-N bond. This is in well agreement with the XPS results which also show that the F-B bonds are stronger compared to the F-N bonds. On further fluorination up to 12.5%, F binds to one of the three B atoms closest to F bonded N atom. For 15.625% of F functionalization, F attaches to next nearest N atom, where F atoms attached to B and N atoms are on opposite sides (fig. S9(E)). The fluorination is found to proceed in the sequence of B and the nearest N instead of random orientation. fig. S9(F)(green circles)shows a plot of the formation energies for different positions of F atoms as a function of F concentration. The negative slope observed in the energy versus concentration plot show that functionalization up to 12.5% of F atoms is indeed thermodynamically favorable. Beyond 12.5% of F concentration, the slope reverses sign, indicating that further fluorination is thermodynamically unfavorable. In this study, the experimental doping concentration was limited to 13.2% F concentration and theoretical data of formation energies commensurate the stability of these structures. We have further performed spin-polarized calculations and found that for 3.125% and 6.25%, the formation energies marked by red triangles in fig. S9(F) remain the same as non-spin-polarized cases. As the concentration of F increases further, the formation energies of spin-polarized systems become lower than non-spin polarized cases (fig. S9(F)). This indicates that fluorination can induce magnetism at higher doping levels.

7a. Alignment of Band edges and band decomposed charge density

In order to understand the non-linearity of fundamental band gap which have been found both theoretically and experimentally from UV spectra analysis, VBM and CBM have been aligned with respect to the vacuum level for each F concentration as shown in fig. S10 (A). Both VBM and CBM decreases as a function of F concentration. Depending on the magnitude of down shift of VBM and CBM, the band gap shows non-linear relationship with F concentration.

Furthermore, the band decomposed charge density has been plotted in order to understand how F concentration plays a role to shift VBM and CBM as shown in fig. S10 (B-C). In pristine BN sheet, VBM and CBM originate from N-p and B-p orbitals, respectively (shown in fig. S10 B). After fluorination, if more number of N atoms contribute to VBM, it shifts below due to its high electronegativity.

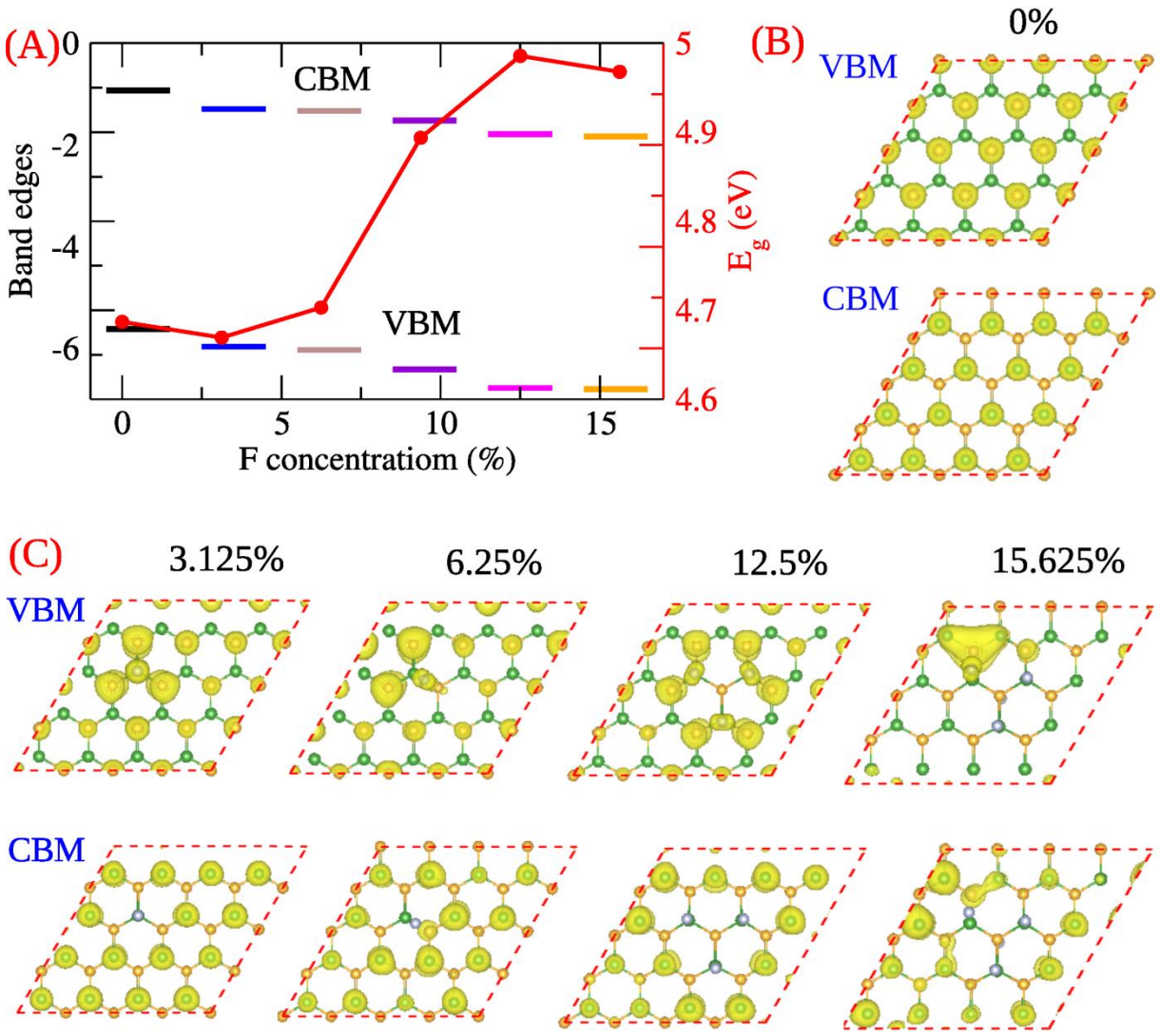

fig. S10. Alignment of band edges and band-decomposed charge density. (**A**) Plots of band edges (VBM and CBM) with respect to vacuum level for FBN systems having different F concentration. The trend of change in fundamental band gap also marked in red line. Band decomposed charge densities are plotted for (**B**) pristine BN sheet and (**C**) FBN having different F concentrations. The isosurface value is considered to be 0.003 e/Å^3 for 15.625% F

concentration and for lower F concentrations and pristine BN sheet, it has been scaled according to the total number of electrons in the system.

In FBN having F concentration of 3.125%, CBM shifts more to lower energy than that of VBM resulting into a decrease in band gap. Due to fluorination, charge densities for VBM become localized near F atoms and therefore, less number of N atoms contribute. Beyond 3.125%, the down shift in VBM is more compared to CBM as the number of contributed N atoms increases with F concentration (shown in fig. S10 C), which leads to increase in band gap till 12.5%. After that, for 15.625%, the number of contributed N atoms reduces, leading to more down shift in CBM compared to VBM resulting into decrease in band gap.

7b. Band Structure

The change in electronic structure upon fluorination on B and N sites have been investigated by comparing the band structures of FBN sheets having 3.125% F concentration with pristine BN sheet. Band structure of completely fluorinated BN sheet is also plotted.

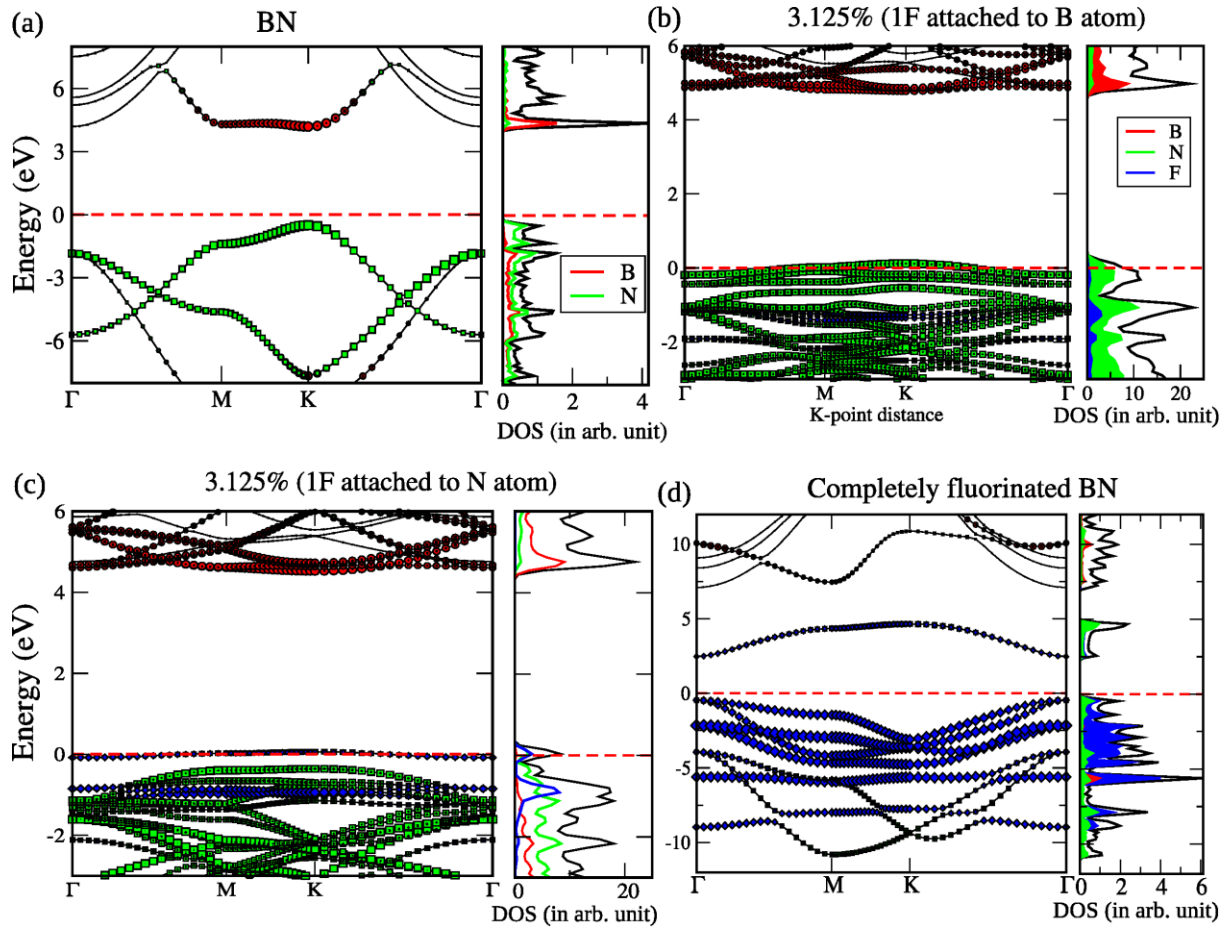

fig. S11. Band structure and density of states of F-BN. (**A**) pristine BN, (**B**) BN sheet with 1F atom attached to B atom (3.125%), (**C**) BN sheet with 1F atom attached to N atom (3.125%) and (**D**) completely fluorinated BN sheets.

7c. Charge accumulation and depletion

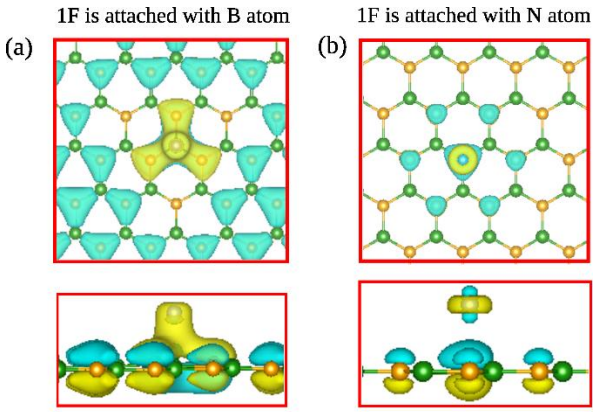

fig. S12. Charge accumulation and depletion of F-BN. with 3.125% F concentration when one F is attached with (**A**) B atom and (**B**) N atom where yellow and sky blue colors denote charge accumulation and depletion respectively. Isosurface value has been taken as 0.017e/A3 for both cases.

Charge accumulation and depletion has been calculated for FBN with 3.125% F concentration when one F atom is attached with B or N atom, using the formula

$$\Delta\rho = \rho_{FBN} - \rho_{BN} - \rho_{F}$$

where, ρ_{FBN}, ρ_{BN} and ρ_{F} denote total charge densities of fluorinated BN having 3.125% F concentration, BN sheet and F atom, respectively. When one F atom is attached with B atom, charge accumulates mainly on B-F bonds, while when F atom is attached with N atom, F atom accumulates less charge compared to that of B-F bond.